Tailor-Made Development of Fast Li Ion Conducting Garnet-Like Solid Electrolytes

Adam Ramzy and Venkataraman Thangadurai*

Department of Chemistry, The University of Calgary, Calgary, Alberta T2N 1N4, Canada

ABSTRACT This paper reports a novel approach to designing advanced solid Li ion electrolytes for application in various solid state ionic devices, including Li ion secondary batteries, gas sensors, and electrochromic displays. The employed methodology involves a solid-solution reaction between the two best-known fast Li ion conductors in the garnet-family of compounds $Li_6BaLa_2M_2O_{12}$ (M = Nb, Ta) and $Li_7La_3Zr_2O_{12}$. Powder X-ray diffraction (PXRD), scanning electron microscopy (SEM), AC impedance, and ^7Li nuclear magnetic resonance (Li NMR) spectroscopy were employed to characterize phase formation, morphology, ionic conductivity, and Li ion coordination in $Li_{6.5}La_{2.5}BaZrMO_{12}$. PXRD shows for formation of a cubic garnet-like structure and AC impedance data is consistent with other known solid Li ion electrolytes. $Li_{6.5}La_{2.5}BaZrTaO_{12}$ exhibits a fast Li ion conductivity of about 6×10^{-3} S cm^{-1} at 100 °C, which is comparable to that of currently employed organic polymer electrolytes value at room temperature. The Nb analogue shows an order of magnitude lower ionic conductivity than that of the corresponding Ta member, which is consistent with the trend in garnet-type electrolytes reported in the literature. Samples sintered at 1100 °C shows the highest electrical conductivity compared to that of 900 °C. ^7Li MAS NMR shows a sharp single peak at 0 ppm with respect to LiCl, which may be attributed to fast migration of ions between various sites in the garnets, and also suggesting average distributions of Li ions at average octahedral coordination in $Li_{6.5}La_{2.5}BaZrMO_{12}$. The present work together with literature used to establish very important fundamental relationship of functional property−Li concentration−crystal structure−Li diffusion coefficient in the garnet family of Li ion electrolytes.

KEYWORDS: Li ion batteries • solid electrolytes • fast Li ion conductors • garnets • $Li_6BaLa_2M_2O_{12}$ (M = Nb, Ta) • AC impedance

1. INTRODUCTION

Among the various modern environmentally oriented areas of alternative energy conversion and storage devices, the development of Li ion secondary (rechargeable) battery has been a top priority because of its high energy density and it is capability for powering everything from microelectronics to hybrid electric cars. Unlike conventional and electrochemical energy systems based on hydrocarbons (e.g., gasoline, methane, methanol), Li ion batteries offer the unique advantage of zero carbon emissions during operation. Although the basic electrochemical principle is same for both fuel cells and batteries, the latter does not require a constant supply of energy source nor does it operate within the galvanic cells. Also, the emission from hydrocarbon-based fuel cells contains greenhouse effect chemical compounds (1−4).

Present Li ion batteries are based mainly on $LiPF_6$ dissolved in polyethylene oxide (PEO) electrolytes, a graphite anode, and a $LiCoO_2$ cathode has several problems due to safety, cost, and durability. Hence, a constant attempt has been made to replace prohibitive cost and toxic $LiCoO_2$ with an alternative environmentally friendly and cheap transition metal oxide electrodes, and the organic polymer electrolytes with solid Li ion conducting electrolytes (SLICEs) because of safety. The SLICE-based Li ion battery enhances cell performance and safety because of high temperature operation and electrochemical stability (1, 2, 5). Also, SLICEs have enormous industrial applications such as electrochromic displays (smart windows), gas sensors (e.g., CO_2, NOx, SOx), and capacitors.

A large groups of layered two-dimensional (2D) and three-dimensional (3D) inorganic SLICEs such as Li_3N; Li-β-alumina; Li_4SiO_4; Li_3PO_4; Li_5MO_4 (M = Al, Ga, Fe); LISICON (lithium superionic conductors, e.g., $Li_{14}ZnGe_4O_{16}$); NASICON-(sodium superionic conductors, e.g., $Na_3Zr_2PSi_2O_{12}$) analogue of Li, i.e., $Li_{1+x}M_{2-x}M_x^{III}PO_{12}$ (M = Ti, Zr, Ge, Hf; M^{III} = Al, In, Sc), (Li,Ln)TiO_3 (Ln = rare earths); $Li_5La_3M_2O_{12}$ (M = Nb, Ta); and Li compound-metal oxide composites have been investigated (5−11). Among them, the earliest work on garnet-related structured $Li_5La_3M_2O_{12}$ (M = Nb, Ta) (11a) and its related compounds show a high Li ion conductivity, chemical stability with Li metal, and high electrochemical stability, which make them a potential candidate for applications in future all-solid-state Li^+ ion batteries. The highest total (bulk + grain-boundary) Li ion conductivities have been reported for $Li_7La_3Zr_2O_{12}$ (11e) and $Li_6La_2BaTa_2O_{12}$ (11f), which display conductibility of 2×10^{-4} and 4×10^{-5} S cm^{-1} at room temperature, respectively.

Subsequent research work has shown that there are many possible substitutions that can be used in order to improve ionic conductivities and also alter the chemical and physical properties of garnet-type lithium ion electrolytes. For examples, O'Callaghan and Cussen showed the possibility of substitutions in both the La and M site to form the compounds $Li_{5+x}Ba_xLa_{3-x}Ta_2O_{12}$ ($0 < x \leq 1.6$) (9). In the present work, using the knowledge of the chemical stability and formation of garnet-like structure (11), we investigate the ionic conductivity of a 1:1 solid solution of $Li_7La_3Zr_2O_{12}$

* Corresponding author. E-mail: vthangad@ucalgary.ca.
Received for review September 22, 2009 and accepted January 14, 2010

DOI: 10.1021/am900643t

and $Li_6La_2BaM_2O_{12}$ (M = Nb, Ta). A key strategy behind this relational synthesis is to understand the effect of chemical substitution at M (Nb or Ta) sites and La sites in the parent $Li_5La_3M_2O_{12}$ phase, and to take advantage of already-known end members' chemical stability against reaction with metallic Li. Here, we report for the first time the synthesis, crystal structure, and Li ion conductivity for $Li_{6.5}La_{2.5}BaZrMO_{12}$. Our results showed that $Li_{6.5}La_{2.5}BaZrMO_{12}$ exhibits comparable bulk Li ion conductivity to that of the two end members, $Li_7La_3Zr_2O_{12}$ and $Li_6La_2BaM_2O_{12}$. Our approach may be extended to design other new ionic conductors and to understand the functional property−chemical composition−structure relationship.

2. EXPERIMENTAL ASPECTS

Compounds of the nominal chemical formula $Li_{6.5}La_{2.5}BaZrMO_{12}$ (M = Nb, Ta) were prepared via a conventional solid-state reaction (ceramic method) using stoichiometric quantities of high-purity $LiNO_3$ (GR, 97%, EM Science), La_2O_3 (99.99%, Alfa Aesar), $Ba(NO_3)_2$ (99+ %, Alfa Aesar), Nb_2O_5 (99.5%, Alfa Aesar), Ta_2O_5 (99%, Alfa Aesar), and ZrO_2 (99+%, Alfa Aesar). The reactants were weighed and ball-milled employing a Pulverisette, Fritsch, Germany ball mill at 200 rpm for 3 h with zirconium balls in 2-propanol. As reported in the garnet-type materials synthesis, 10 wt % excess $LiNO_3$ was added to account for loss of lithium oxide during sintering (11−16). After mixing and drying at room temperature, samples were heated at 800 °C to decompose the metal salts. Samples were then reground for 5 h and powder samples were pressed into pellets under isostatic pressure. Pellets were sintered at 900 and 1100 °C for 5−6 h. Powder X-ray diffraction (PXRD; Bruker D8 powder X-ray diffractometer (CuKα, 40 kV, 40 mA)) was employed for phase formation characterization. After confirmation of successful a single-phase garnet-type structure, pellets were painted with Au electrodes (paste, cured at 600 °C for 1 h) for electrical conductivity employing Solarton SI 1260 impedance and gain-phase analyzer in the frequency range of 0.01 to 10×10^6 Hz in air. ^{7}Li magic angle spinning (MAS) nuclear magnetic resonance (NMR) (Bruker AMX 300) was performed on powdered $Li_{6.5}La_{2.5}BaZrMO_{12}$ samples with a spinning frequency of 5 kHz and chemical shift values were expressed against solid LiCl.

3. RESULTS AND DISCUSSION

Figure 1 shows the experimental and calculated powder X-ray diffraction (PXRD) patterns of $Li_{6.5}La_{2.5}BaZrNbO_{12}$ and $Li_{6.5}La_{2.5}BaZrTaO_{12}$ based on Cussen model of $Li_{5+x}Ba_xLa_{3-x}Ta_2O_{12}$ ($0 < x \leq 1.6$) (9) and Slater group model of a simple body centered cubic for $Li_6La_2ANb_2O_{12}$ (A = Alkaline earth ions) (16). We have indexed the PXRD patterns (peaks intensity above 10%) on a garnet-like cell constants of a = 12.815(4) Å for Nb member and a = 12.783(4) Å for the Ta compound (see Table S1 in the Supporting Information). Cussen used neutron diffraction and showed that Li ions exist in not only the distorted octahedral site (48g) but also the tetrahedral (24d) site in the space group ($Ia\bar{3}d$) for the parent phase $Li_5La_3Ta_2O_{12}$[10] and Ba-doped $Li_{5+x}Ba_xLa_{3-x}Ta_2O_{12}$ (9). Also, they have suggested roughly a 33% vacancy in the 48g sites and a 66% vacancy in the 24d sites in the parent $Li_5La_3M_2O_{12}$ phase (10). Because of the distorted octahedral arrangements, the Li - Li distance was found to exhibit a wide range of 1.500(15)−2.381(11) Å. It has also been proposed, that the tetrahedral 24d sites merely act to lock in the Li ions, whereas the octahedral sites cations are quite free (16). Through the realization of the importance of the octahedral site Li ions and the low occupancy, we proposed our new compounds, which show near identical garnet-like crystal structure, but with more lithium ions that may take the empty 48g sites in the space group ($Ia\bar{3}d$). Our samples appear not to show additional diffraction lines due to tetragonal symmetry structure, as reported recently for $Li_7La_3M_2O_{12}$ (M = Zr, Sn) (12, 17). Slater group has prepared polycrystalline tetragonal symmetry Sn-containing garnet at low temperature (900 °C) and cubic polymorph by rapid cooling (12), and Awaka et al. prepared a tetragonal $Li_7La_3Zr_2O_{12}$ by single-crystal growth (12). It is important to mention that Murugan et. al stabilized cubic polycrystalline $Li_7La_3Zr_2O_{12}$ by conventional solid-state reaction at high temperature (1200 °C) (11e). Accordingly, the preparation

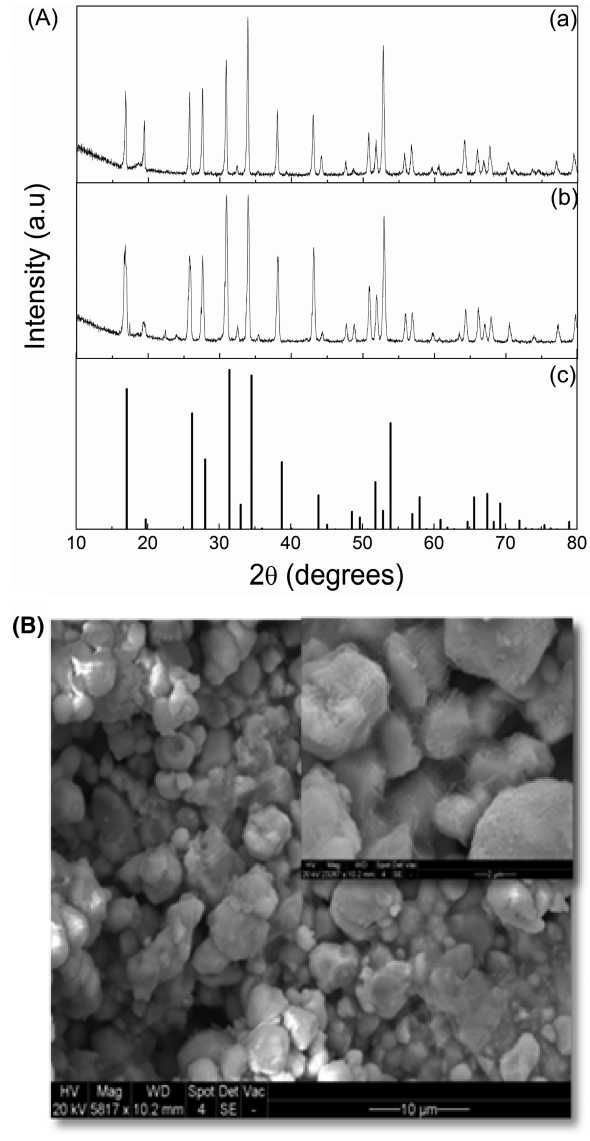

FIGURE 1. (A) Powder X-ray diffraction patterns of $Li_{6.5}La_{2.5}BaZrMO_{12}$: (a) M = Ta, (b) M = Nb and (c) calculated on the basis of the atomic coordinates of $Li_{5+x}Ba_xLa_{3-x}Ta_2O_{12}$ (x = 1) (9). We see that both calculated and measured data are akin to each other, and confirm the formation of garnet-type structure. (B) Typical SEM images (10 μm) of powdered $Li_{6.5}La_{2.5}BaZrTaO_{12}$ prepared at 900 °C in air for 24 h. Inset shows data at 2 μm scale.

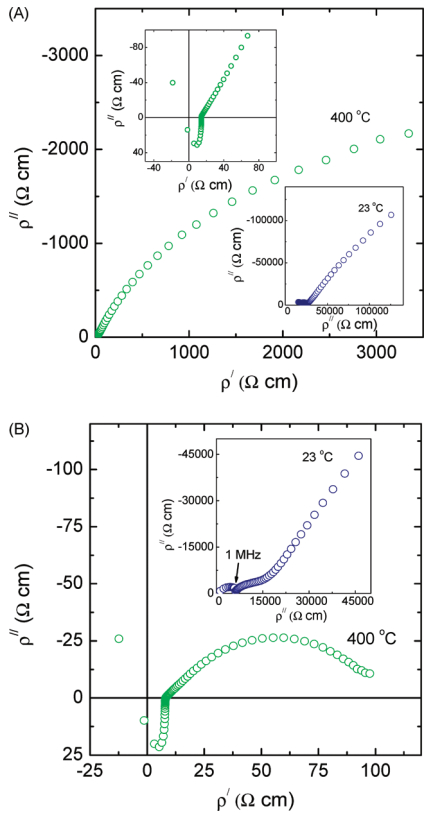

FIGURE 2. AC impedance of $Li_{6.5}La_{2.5}BaZrTaO_{12}$ at 23 and 400 °C: (a) sample prepared at 900 °C and (b) prepared at 1100 °C in air for 24 h. A tail at low-temperature and at low-frequency side may be ascribed to Li ion-blocking Au electrodes. A spike at 1 MHz is marked and can be attributed to instrumental artifact. The positive imaginary value at high temperatures is observed as a result of inductance. Inset in (a) shows expanded region of impedance data at 400 °C.

condition such as heating and cooling rates and sintering temperature appear to be very important in stabilization of different polymorphs of the garnet-type family of materials.

In Figure 2, we show typical AC impedance plots at 23 and 400 °C of $Li_{6.5}La_{2.5}BaZrTaO_{12}$ prepared at 900 and 1100 °C, which shows mainly bulk and electrode contributions. A similar impedance plots was observed for the corresponding Nb compound $Li_{6.5}La_{2.5}BaZrNbO_{12}$. The shape of the impedance plot is consistent with other garnet-type electrolytes reported in the literature (11, 17). The low-frequency side intercept to the real axis was used to calculate the bulk ionic conductivity. However, at high temperatures, the interpretation of impedance data becomes more complex because of the high-frequency imaginary impedance values becoming positive. This is due to the contributions of cables, furnaces, and electrochemical cells leads, and the effect becomes especially prevalent when the samples are conducting very strongly. Thus, we feel that these experimental limitations will control the impedance measurements and accordingly, the reported conductivity of the samples may not represent the actual conductivity. Also, the contribution because of empty cell lead resistance was not subtracted, which may have an effect on reported conductivity results. Further 4-probe DC electrical conductivity measurements may be required to determine the actual conductivity of the samples.

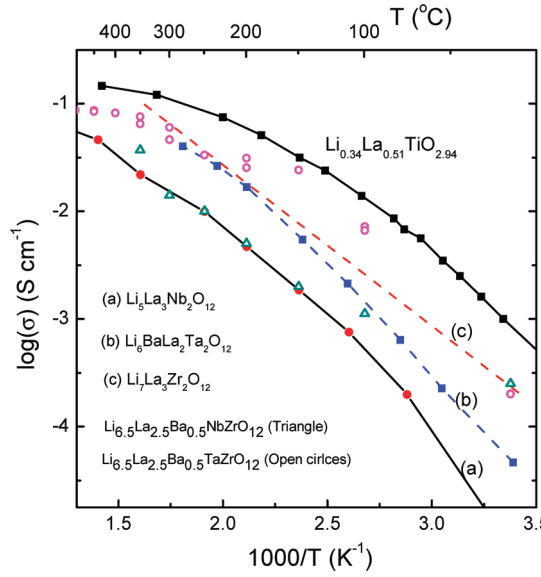

FIGURE 3. Arrhenius plots for electrical conductivity of $Li_{6.5}La_{2.5}BaZrMO_{12}$ (M = Nb (open triangles); Ta (open circles) prepared at 1100 °C. For purpose of comparison, Li ion conductivity extracted from literature $Li_5La_3Nb_2O_{12}$ (11a), $Li_6La_2BaTaO_{12}$ (11d,f), and $Li_7La_3Zr_2O_{12}$ (11e) is included. The electrical conductivity of the presently investigated 1:1 solid solution $Li_{6.5}La_{2.5}BaZrMO_{12}$ samples is comparable to that of end members.

Shown in Figure 3 is the Arrhenius plot for the bulk Li ion conductivity of the garnet-like structure $Li_{6.5}La_{2.5}BaZrMO_{12}$ prepared at 1100 °C. The data obtained during the heating and cooling cycle follow on the same line, indicating a thermal equilibrium behavior. In Table S2 (see the Supporting Information), we list the bulk ionic conductivity as a function of temperature of $Li_{6.5}La_{2.5}BaZrTaO_{12}$ sintered at 900 and 1100 °C for different trials. The electrical conductivity data was found to be nearly the same within the errors of the experiment between two different trials (see Table S2 in the Supporting Information). The slight difference may be due to difference in thermal equilibrium and or stability of the temperature due to the function of the furnace. Samples prepared at 1100 °C showed a slightly higher bulk Li ion conductivity compared to that of samples obtained at 900 °C. A similar behavior was reported for $Li_5La_3Nb_2O_{12}$ and In- and K-doped $Li_5La_3Nb_2O_{12}$ (18). The increase in the electrical conductivity was explained due to an increase in the size of the particles from a high sintering temperature and better particle to particle contact (18). It also could be due to change in the mobile Li ion concentrations as a result of sintering at elevated temperatures. We see the conductivity of the investigated $Li_{6.5}La_{2.5}BaZrMO_{12}$ is comparable to the two end members, $Li_6La_2BaM_2O_{12}$ and $Li_7La_3Zr_2O_{12}$ (11). The activation energy for ionic conductivity was found to be 0.31 eV which is close agreement with other members reported in the garnet-type lithium ion conductors (11). The Nb analogue $Li_{6.5}La_{2.5}BaZrNbO_{12}$ exhibits about an order of magnitude lower bulk conductivity than the corresponding Ta member, especially at high temperature, which is in agreement with the data reported for $Li_6La_2BaM_2O_{12}$ (M = Nb, Ta) (11f, 11g).

Since the first garnet-type lithium ion conductor was introduced in 2003 by Thangadurai et al. (11a), several

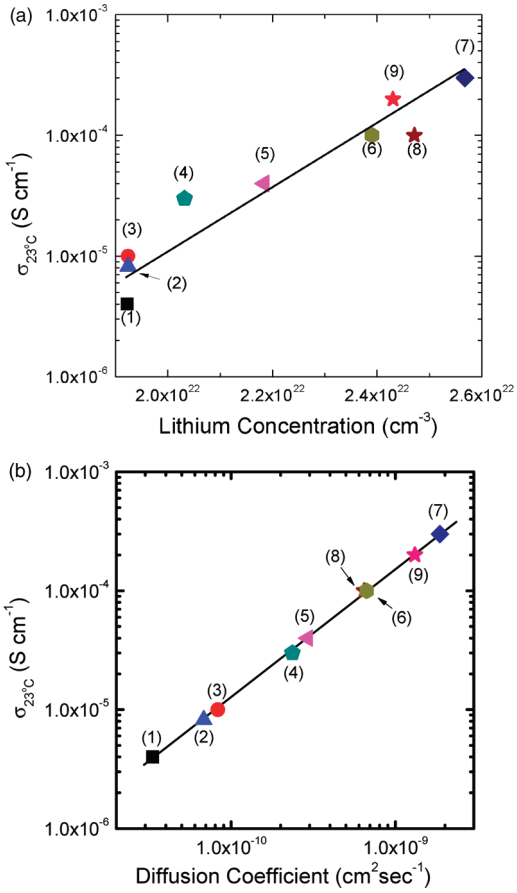

FIGURE 4. (a, b) Variation in electrical conductivity as a function of Li concentrations and electrical conductivity vs diffusion coefficients of garnet-type compounds. (1) $Li_5La_3Ta_2O_{12}$ (11a), (2) $Li_5La_3Sb_2O_{12}$ (11b), (3) $Li_5La_3Nb_2O_{12}$ (11a), (4) $Li_{5.5}BaLa_2Ta_2O_{11.75}$ (11c), (5) $Li_6La_2BaTaO_{12}$ (11d), (6) $Li_{6.5}BaLa_2Ta_2O_{12.25}$ (11c), (7) $Li_7La_3Zr_2O_{12}$ (11e), (8) $Li_{6.5}La_{2.5}Ba_{0.5}TaZrO_{12}$, 900 °C (present work), (9) $Li_{6.5}La_{2.5}Ba_{0.5}TaZrO_{12}$ 1100 °C (present work). The line passing through the data points is guide to eye.

authors (8−13) have worked on this family of compounds to understand the chemical composition−crystal structure−ionic conductivity relationship. The conductivity (σ) and concentration (n) of mobile species can be related simply by the expression: $\sigma = |z_{Li}|N_{Li}q\mu_{Li}$ (where q is the elementary charge (1.6×10^{-19} C), z is the valence (for Li, $z = +1$), and μ is the electrical mobility of Li ions). Examples of successful increases in conductivity through an increase in n has arisen in $Li_6ALa_2M_2O_{12}$ (A = Ca, Sr, Ba; M = Nb, Ta) (11f, 11g) compounds and especially in $Li_7La_3Zr_2O_{12}$ (11e). The concentrations of Li in various garnet-type lithium ion conductors was found to vary linearly with log (conductivity) (Figure 4a), which confirms that lithium content play critical role in ionic conductivit y (11a, 11d, 11e). However, a major concern in such a simple explanation occurs for chemical substitutions in either of the M or Nb sites such as $Li_5La_3M_2O_{12}$ (M = Nb, Ta, Sb) (12). Using the same equation, we see that the only other variable that can be manipulated to increase Li ion conductivity is the electrical mobility (μ) which can be related to the component diffusion coefficient of Li (D). These two are related by the Nernst−Einstein equation, $\mu = qD/kT$, where k is the Boltzmann constant and T is the absolute temperature. Indeed, we see that the

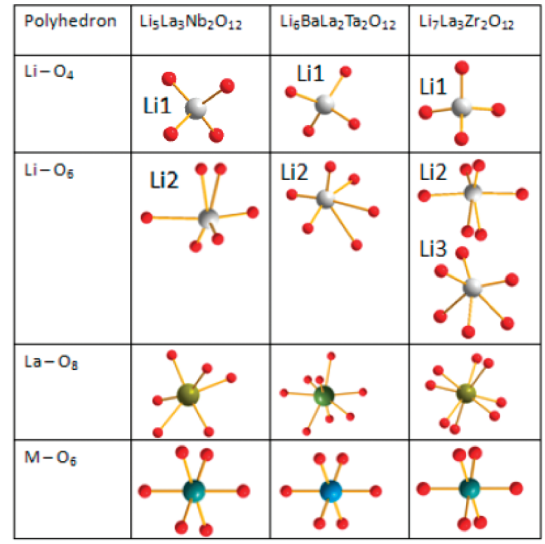

FIGURE 5. Idealized Li−O, La−O, and M−O polyhedral in $Li_5La_3Nb_2O_{12}$ (10), $Li_6La_2BaTaO_{12}$ (9), and $Li_7La_3Zr_2O_{12}$ (17) phases.

diffusion coefficient obtained from the bulk ionic conductivity was found to be linear (in log plot) among the various types of selected garnet-type solid electrolytes (Figure 4b). This expression may be used to explain the changes in conductivity as a result of metal substitutions in $Li_5La_3M_2O_{12}$, but the changes in ionic conductivity due to microstructure and preparation method cannot be easily explained. This distinction in conductivity may arise because of several factors, including bulk and grain-boundary contributions as a result of particle to particle contact, density, sintering, and electrode to electrolyte interface effect.

Recent work has also shown the effect of d^0 and d^{10} cations substitution in the garnet structure on Li ion conductivity. Also, the percentage of Li ions at the various crystallographic positions, including tetrahedral and octahedral pays crucial role in ionic conductivity. Cussen and Yip reported that the increase in lattice parameters of garnet type $Li_5La_3Sb_2O_{12}$ when a d^0 cation such as W^{VI} is substituted for d^{10} Sb^V (19). Substitution of W^{VI} for Sb^V in $Li_5La_3Sb_2O_{12}$ decreases not only lithium content and also changes distribution of lithium coordination. All the Li ions are occupied in only tetrahedral sites in $Li_3Nd_3W_2O_{12}$, whereas they are distributed in both tetrahedral and octahedral sites in $Li_5La_3Sb_2O_{12}$ (19). Furthermore, substitution of Te^{VI} for Nb/Ta in $Li_5La_3M_2O_{12}$ decreased the ionic conductivity by several orders of magnitude because the Li ions occupy the tetrahedral sites, and all the octahedral sites are 100% empty (13). The migration of Li ions from tetrahedral sites to octahedral sites creates major compression of Li^+ ion before migration into the empty holes because of LnO and MO polyhedrons. Although the concentration of Li ions in the investigated Nb and Ta members and lattice constant are nearly the same, the higher ionic conductivity of latter member cannot be described using the empirical conductivity relationship. This may be attributed to change the symmetry of compounds, hence detailed neutron diffraction or

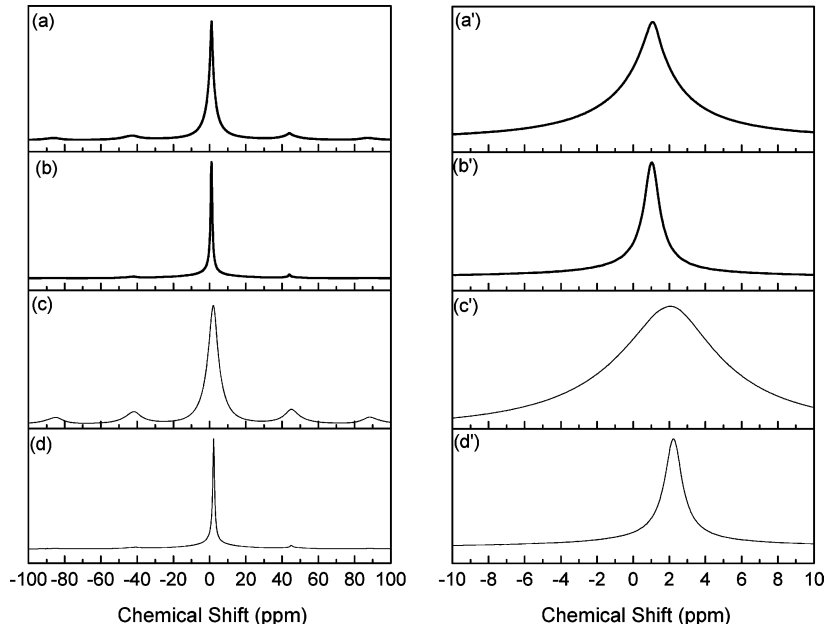

FIGURE 6. ^{7}Li MAS NMR of $Li_{6.5}La_{2.5}BaMZrO_{12}$ [M = Nb(c,d), Ta(a,b)]. samples a and c were sintered at 900 °C and samples b and d were sintered at 1100 °C in air. In a′−d′, we show the data at the expanded region. Chemical shift values were expressed with respect to solid LiCl.

single-crystal structure study is invoked to explain the ionic conductivity behavior of the presently investigated compounds.

In Figure 5, we show the various metal−oxygen coordinations in $Li_5La_3Nb_2O_{12}$, $Li_6La_2BaTa_2O_{12}$, and $Li_7La_3Zr_2O_{12}$ phases. The occupation of Li ions in 4 or 6-fold coordination can be controlled by the nature of M-site cations in the garnet-type structure. The present and literature (10−14) studies showed that such a control on Li ion occupancy is very important in ionic conductivity of the garnet-like structure compounds. In order to verify the various sites of the Li in the garnet-like structure, ^{7}Li MAS NMR was performed for $Li_{6.5}La_{2.5}BaZrMO_{12}$ prepared at 900 and 1100 °C, and chemical shift values were expressed against solid LiCl (Figure 6). ^{7}Li NMR has been used to great success in determining the Li dynamics in lithium containing solid electrolytes and electrode materials and to investigate the Li and oxygen coordination in solid-state materials (21−30). For example, Xu et al., showed three different co-ordination sites for Li in crystalline lithium orthosilicate Li_4SiO_4 using ^{7}Li MAS NMR (23). However, the chemical shift values for these three types of Li−O coordination was found to be in a narrow range of − 2 to + 1.5 ppm. The present work and previous authors' work shows a single peak at a chemical shift value between 0 and 3 ppm (13, 21, 29). Samples sintered at 1100 °C show sharp peak compared to that of the corresponding 900 °C samples, which aligns with the conductivity trend (Figures 2 and 3). Neutron diffraction analysis of the Li-excess $Li_{5+x}Ba_xLa_{3-x}Ta_2O_{12}$ ($0 < x < 1.6$) showed that lithium ions occupy three different types of sites, including the tetrahedral, octahedral and distorted octahedral in the garnet-like structure (9). The Li−Li distance between the octahedron in $Li_{6.6}Ba_{1.6}La_{1.4}Ta_2O_{12}$ was found be in the range of 2.471(12) Å (9), which was further confirmed in other garnet-like $Li_{6.4}Sr_{1.4}La_{1.6}M_2O_{12}$ (M = Sb, Ta) (31). The repulsion caused by the short Li−Li atom distance and partial occupation of Li ions at various interstitial sites in the garnets appears to resulting a fast ionic conductivity. Because of a large overlap of ^{7}Li MAS NMR signals, we were unable to distinguish LiO_4 and LiO_6 units in the presently investigated garnet-type materials.

It is important to mention that our ^{7}Li MAS NMR data was found to be comparable to that of Wullen et al. (27) and Koch et al. (29) results. However, a detailed variable-temperature NMR study is invoked to establish the Li ion dynamics in the presently investigated garnet-like 1:1 solid solution compounds. The bond valence analysis of the parent structured $Li_5La_3M_2O_{12}$ showed three-dimensional networks of energetically equivalent partially occupied sites around MO_6 is available for ionic conduction (20). The number of accessible equivalent Li sites is more than 20% higher than the number of occupied sites, and an extended region of low bond valence sum mismatch centered by a vacant tetrahedral coordinated Li site enhances the conductivity (20). It is also important to mention here that the dramatically increased conductivities of solid solution $Li_{4-3x}Al_xSiO_4$ are due to a decrease in the Li ion occupation at particular interstitial sites; at $x = 0.5$, such sites are completely empty (15). The study on the present garnet-like and $Li_{4-3x}Al_xSiO_4$ showed clearly that the Li ion content and their sites in the structure is critical for fast ionic conduction.

4. CONCLUSIONS

In summary, 1:1 solid-solution compound $Li_{6.5}La_{2.5}BaZrTaO_{12}$ exhibits fast Li ion conductivity on the order of 10^{-3} S/cm^{-1} at 100 °C, which is comparable to that of currently employed organic polymer electrolytes in Li ion secondary batteries. Samples sintered at 1100 °C shows higher electrical conductivity compared to that of the corresponding 900 °C compound. ^{7}Li MAS NMR shows a single peak at 0 ppm,

which seems to be attributed to the distribution of Li ions at the average octahedral coordination in $Li_{6.5}La_{2.5}BaZrMO_{12}$ for both 900 and 1100 °C sintered samples. However, variable-temperature NMR study is required to understand the dynamics and coordination of Li ions in the investigated solids. Furthermore, increase the Li content in the parent compound $Li_5La_3M_2O_{12}$ by aliovalent substitution at the La by larger Ba-atom and M-sites by polarizable cations appear to be the best choice for high ionic conduction. Our earlier work (11) showed that the Ta- and Zr-containing garnet-type compound exhibit a high electrochemical and chemical stability against reaction with metallic Li, hence the investigated new Ta and Zr member has a great potential to find applications in solid-state batteries as well as other ionic devices.

Acknowledgment. This research work is supported by the AUTO21 Network of Centres of Excellence, Canada's national automotive research and development program.

Note Added after ASAP Publication. In the original version of this paper published to the web on January 27, 2010, there were several incorrect chemical formulas. The revised version was published on February 1, 2010. Additional corrections were made to chemical formulas and the revised paper was published on February 4, 2010.

Supporting Information Available: Indexed powder X-ray data and electrical conductivity (PDF). This material is available free of charge via the Internet at http://pubs.acs.org.

REFERENCES AND NOTES

(1) Tarascon, J.; Armand, M. *Nature* **2001**, *414*, 359–367.
(2) Dell, R. *Solid State Ionics* **2000**, *134*, 139–158.
(3) Vincent, C. *Solid State Ionics* **2000**, *134*, 159–167.
(4) (a) Owen, J. *Chem. Soc. Rev.* **1997**, *26*, 259–267. (b) Song, J.; Wang, Y.; Wan, C. *J. Power Sources* **1999**, *77*, 183–197. (c) Armand, M.; Endres, F.; MacFarlane, D.; Ohno, H.; Scrosati, B. *Nat. Mater.* **2009**, *8*, 621–629. (d) Goodenough, J.; Kim, Y. *Chem. Mater.* **2010**, 587–603.
(5) Kendrick, E.; Slater, P. *Annu. Rep. Prog. Chem., Sect A* **2009**, *105*, 436–459.
(6) (a) Imanaka, N.; Adachi, G. *Acc. Chem. Res.* **1994**, *27*, 265–270. (b) Adachi, G.; Imanaka, N.; Aono, H. *Adv. Mater.* **1996**, *8*, 127–135. (c) Thangadurai, V.; Weppner, W. *Ionics* **2006**, *12*, 81–104. (d) Knauth, P. *Solid State Ionics* **2009**, *180*, 911–916.
(7) Stramare, S.; Thangadurai, V.; Weppner, W. *Chem. Mater.* **2003**, *15*, 3974–3990.
(8) Robertson, A. D.; West, A. R.; Ritchie, A. G. *Solid State Ionics* **1997**, *104*, 1–11.
(9) O'Callaghan, M. P.; Cussen, E. J. *Chem. Commun.* **2007**, 2048–2050.
(10) Cussen, E. J. *Chem Commun.* **2006**, 412–413.
(11) (a) Thangadurai, V.; Kaack, H.; Weppner, W. *J. Am. Ceram. Soc.* **2003**, *86*, 437–440. (b) Percival, J.; Kendrick, E.; Slater, P. *Solid State Ionics* **2008**, *179*, 1666–1669. (c) Murugan, R.; Thangadurai, V.; Weppner, W. *Appl. Phys. A: Mater. Sci. Process.* **2008**, *91*, 615–620. (d) Thangadurai, V.; Weppner, W. *J. Power Sources.* **2005**, *142*, 339–344. (e) Murugan, R.; Thangadurai, V.; Weppner, W. *Angew. Chem., Int. Ed.* **2007**, *46*, 7778–7781. (f) Thangadurai, V.; Weppner, W. *Adv. Funct. Mater* **2005**, *15*, 107–112. (g) Thangadurai, V.; Weppner, W. *J. Am. Ceram. Soc.* **2005**, *88*, 411–418.
(12) Percival, J.; Kendrick, E.; Smith, R.; Slater, P. *Dalton Trans.* **2009**, *35*, 5177–5181.
(13) O'Callaghan, M.; Powell, A.; Titman, J.; Chen, G.; Cussen, E. J. *Chem. Mater.* **2008**, *20*, 2360–2369.
(14) O'Callaghan, M. P.; Lynham, D.; Cussen, E. J.; Chen, G. *Chem. Mater.* **2006**, *18*, 4681–4689.
(15) Whitacre, J.; West, W. *Solid State Ionics* **2004**, *175*, 251–255.
(16) Percival, J.; Slater, P. *J. Solid State Commun.* **2007**, *142*, 355–357.
(17) Awaka, J.; Kijima, N.; Hayakawa, H.; Akimoto, J. *J. Solid State Chem.* **2009**, *182*, 2046–2052.
(18) Thangadurai, V.; Weppner, W. *J. Solid State Chem.* **2006**, *179*, 974–984.
(19) Cussen, E. J.; Yip, T. *J. Solid State Chem.* **2007**, *180*, 1832–1839.
(20) Thangadurai, V.; Adams, S.; Weppner, W. *Chem. Mater.* **2004**, *16*, 2998–3006.
(21) Smaihi, M.; Petit, D.; Korb, J. P.; Boilot, J. P. *J. Solid State Chem.* **1991**, *94*, 260–273.
(22) Cocciantelli, J. M.; Suh, K. S.; Senegas, J.; Doumerc, J. P.; Pouchard, M. *J. Phys. Chem. Solids* **1992**, *53*, 57–59.
(23) Xu, Z.; Stebbins, J. F. *Solid State Nucl. Magn. Reson.* **1995**, *5*, 103–112.
(24) M.P.J. Peeters, M. P. J.; van Bommel, M. J.; Neilen-ten Wolde, P. M. C.; van Hal, H. A. M.; Keur, W. C.; Kentgens, A. P. M. *Solid State Ionics* **1998**, *112*, 41–52.
(25) Nagel, R.; Ch. Wickel, Ch.; Senker, J.; Lutz, H. D. *Solid State Ionics* **2000**, *130*, 169–173.
(26) Cahill, L. S.; Chapman, R. P.; Britten, J. F.; Goward, G. R. *J. Phys. Chem. B* **2006**, *110*, 7171–7177.
(27) Wullen, L. V.; Echelmeyer, T.; Meyer, H. W.; Wilmer, D. *Phys. Chem. Chem. Phys.* **2007**, *9*, 3298–3303.
(28) Maldonado-Manso, P.; Martín-Sedeño, M. C.; Bruque, S.; Sanz, J.; Losilla, E. R. *Solid State Ionics* **2007**, *178*, 43–52.
(29) Koch, B.; Vogel, M. *Solid State Nucl. Magn. Reson.* **2008**, *34*, 37–43.
(30) Cahill, L. S.; Kirby, C. W.; Goward, G. R. *J. Phys. Chem. C* **2008**, *112*, 2215–2221.
(31) O'Callaghan, M. P.; Cussen, E. J. *Solid State Sci.* **2008**, *10*, 390–395.

AM900643T